THE ASTROPHYSICAL JOURNAL, 298:147–160, 1985 November 1

X-RAY PULSAR MODELS. I. ANGLE-DEPENDENT CYCLOTRON LINE FORMATION AND COMPTONIZATION

P. MÉSZÁROS
Astronomy Department, Pennsylvania State University
AND
W. NAGEL
Max-Planck-Institut für Physik und Astrophysik, Institut für Astrophysik
Received 1985 February 25; accepted 1985 May 2

ABSTRACT

We calculate spectra and cyclotron line shapes of static X-ray pulsar atmospheres with slab and column geometry, including internal thermal sources and external illumination. We do this utilizing a multiangle, incoherent scattering formalism, which yields pulse-phase spectroscopic information. The comparison with observations of integrated spectra and of phase-dependent cyclotron line properties indicates a better fit for the slab models.

Subject headings: line profiles — pulsars — radiative transfer — X-rays: binaries

I. INTRODUCTION

Most of the information we have about X-ray pulsars consists of spectra and pulse shapes. For many objects this has been refined to the point where the spectrum as a function of spin phase is available (e.g., White, Swank, and Holt 1983; Voges *et al.* 1982; Rose *et al.* 1979; Pravdo *et al.* 1978). The other observational feature which plays a key role for its physical importance, if not its ubiquity, is the cyclotron line seen in Her X-1 (Trümper *et al.* 1978) and in 4U 0115+63 (Wheaton *et al.* 1979; Rose *et al.* 1979; White, Swank, and Holt 1983).

Early attempts at understanding theoretically the spectra of X-ray pulsars neglected Comptonization and used the diffusion approximation for simplicity (Ventura, Nagel, and Mészáros 1979; Nagel 1980; Mészáros, Nagel, and Ventura 1980; Kirk and Mészáros 1980; Kaminker, Pavlov, and Shibanov 1982). Other investigations included Comptonization, while leaving out anisotropy effects (Bonazzola, Heyvaerts, and Puget 1979; Wasserman and Salpeter 1980; Nagel 1981*b*). On the other hand, anisotropy effects, which determine the pulse profiles, were studied mostly neglecting Comptonization (Kanno 1980; Nagel 1981*a*; Mészáros and Bonazzola 1981; Kaminker, Pavlov, and Shibanov 1982; Mészáros *et al.* 1983; Harding *et al.* 1984). It is, however, evident from the strong angle and frequency dependence of the cross sections in a strong magnetic field (Canuto, Lodenquai, and Ruderman 1971; Ventura 1979; Mészáros and Ventura 1978) that frequency changes are strongly coupled to angle variations. With the Monte Carlo method (Yahel 1979, 1980; Pravdo and Bussard 1981) one can, in principle, study both anisotropy and Comptonization effects, but in practice this method is useful only at low optical depths, i.e., in the continuum below the resonance, but not near the resonance.

The approach we employ here is a difference method for solving the radiative transfer equation, the so-called Feautrier method (Mihalas 1978). Using the approximate transfer equations for the two polarization modes (Gnedin and Pavlov 1974), the Feautrier method was first applied to the transfer problem in strongly magnetized plasma by Nagel (1981*a*, *b*). In those calculations Comptonization and anisotropy effects were separately studied by making simplifying assumptions: either that of coherent scattering (Nagel 1981*a*), or the two-stream approximation (Nagel 1981*b*).

In this paper, we want to abandon these drastic simplifications and use the Feautrier method to study the combined effects of anisotropy and Comptonization. We are thus able to obtain phase-dependent spectra, of both the continuum and the line, including Comptonization. We also allow for external photon sources illuminating the inner or outer boundaries. Examples considered are an arbitrary input at the inner boundary, e.g., from the neutron star surface, or alternatively, a soft photon source at the outside boundary, due, e.g., to a disk or the Alfvén surface.

In § II we discuss the photon creation and scattering process in a tenuous plasma in a field of $B \gtrsim 10^{12}$ G and discuss the evaluation of the redistribution function in angle, frequency, and polarization. The method of solution of the magnetic Feautrier equations with the new boundary conditions is treated in § III. We present the numerical results in § IV and evaluate these models within the astrophysical context in § V, comparing them with some of the available observations.

II. VACUUM AND THERMAL EFFECTS ON THE POLARIZATION MODES

In calculations that have been published so far, the vacuum, thermal, and incoherent scattering effects were not treated together. Thus Mészáros and Ventura (1978, 1979) and Gnedin, Pavlov, and Shibanov (1978) discussed vacuum effects in the cold plasma, coherent scattering approximation. Wasserman and Salpeter (1980) discussed incoherent transfer ignoring polarization effects. Vacuum and thermal effects were taken into account by Kirk and Mészáros (1980) and Pavlov, Shibanov, and Yakovlev (1980), while Comptonization was ignored. Nagel (1981*b*) used thermal polarization modes with first-order incoherent scattering effects but neglected vacuum polarization. Such simplifications were necessary in the earlier analyses, in order to disentangle the various effects and achieve a piecemeal understanding of a complicated problem. It now appears at this stage necessary, if one wants to approach the

full physical situation, to include vacuum, thermal, and incoherent scattering effects all together in the same calculation.

The differential scattering cross section in a strong magnetic field (Nagel 1981*b*) is

$$\frac{d^2\sigma}{d\omega' d\Omega'}(\omega'\theta' \leftarrow \omega\theta) = r_0^2 \frac{\omega'}{\omega} \int dp f(p) |\langle e'| \Pi |e\rangle|^2 \delta(\omega + \Delta\omega - \omega') \,. \quad (1)$$

Here r_0 is the classical electron radius, ω, ω' are the photon frequencies before and after the scattering, θ, θ' their directions, and e, e' the polarization vectors of the photons, and $r_0\ \Pi$ is the scattering amplitude. The electron momentum distribution $f(p)$ is taken, as in previous calculations, to be a one-dimensional Maxwellian for electrons in the lowest ($n = 0$) Landau level. Energy and (z-)momentum conservation laws give $\Delta\omega = p^2/2 - p'^2/2 = p\Delta k - \Delta k^2/2$, $\Delta k = k' - k = \omega' \cos\theta' - \omega \cos\theta$. Here k is the photon momentum along the magnetic field, and $\hbar = c = m = 1$. These expressions are nonrelativistic but include quantum corrections leading to the recoil term in the resonant denominator of the scattering amplitude. The relativistic expressions allow the study of higher temperatures and higher harmonics (Mészáros, Nagel, and Bussard 1984), but for $kT \ll \hbar\omega_B$ the first-order corrections are more convenient for investigating the ground harmonic and the continuum. The polarization modes e_1, e_2 are

$$|e_1\rangle = \cos\psi\,|a\rangle + i \sin\psi\,|b\rangle \,,$$
$$|e_2\rangle = \sin\psi\,|a\rangle - i \cos\psi\,|b\rangle \,, \quad (2)$$

where

$$|a\rangle = \begin{pmatrix} -\cos\theta \\ 0 \\ \sin\theta \end{pmatrix}, \quad |b\rangle = \begin{pmatrix} 0 \\ 1 \\ 0 \end{pmatrix}, \quad (3)$$

and

$$\tan 2\psi = \frac{1}{b} = \frac{2\cos\theta}{\sin^2\theta} \frac{T_+ - T_-}{2T_z - T_+ - T_-} \,, \quad (4)$$

and T_+, T_-, T_z are integrals over the electron momenta of the forward scattering amplitudes. The quantity b in equation (4) is related to the ellipticity of the polarization modes. In the cold plasma limit one recovers $b \approx (\omega_B/\omega) \sin^2\theta/2 \cos\theta$. The vacuum correction in this limit is (Mészáros and Ventura 1979) $b \rightarrow b[1 + V(\omega^2 - \omega_B^2)/\omega_B^2]$, where

$$V = (\alpha/15\pi)(B/B_c)^2(\omega/\omega_p)^2 \quad (5)$$

measures the influence of the virtual e^+e^- pairs in the strong magnetic field relative to the real electrons of the plasma. Here B_c is the field at which the Landau level spacing equals the electron rest mass energy, $B_c = m^2c^3/e\hbar = 4.414 \times 10^{13}$ G, and α is the fine structure constant. In a hot plasma the vacuum correction is obtained in a similar manner (Kirk 1980). In equation (4) it is equivalent to replacing T_z by $T_z - V$, so that equation (4) reads

$$\tan 2\psi = \frac{2\cos\theta}{\sin^2\theta} \frac{T_+ - T_-}{2(T_z - V) - (T_+ + T_-)} \,. \quad (6)$$

Here the $T_{+,-,z}$ include the first-order relativistic and quantum corrections, being equal to the $\Pi_{+,-,z}$ terms specialized to $\omega' = \omega$, $k' = k$ (Nagel 1981*b*).

A plot of the differential scattering cross section $d^2\sigma/d\omega d\Omega$ is given in Figure 1, where we compare the values with and without vacuum polarization. The values without vacuum effects agree with those of Nagel (1981*b*), except for a factor of $(4\pi)^{-1}$ which was erroneously omitted in Figure 1 of that paper. With vacuum polarization included, the differential cross section depends also on the density, which was chosen to be $\rho = 1.67 \times 10^{-4}$ g cm^{-3}, and $kT = 10$ keV, $\omega_B = 38$ keV. For the vacuum case, Figure 1*b*, note the jump of the cross section for some angles at the "second vacuum frequency" $\omega_{v2} \approx \omega_B$, almost coincident with the laboratory frame cyclotron frequency. A similar jump in the opposite direction also occurs at the "first vacuum frequency" $\omega_{v1} \approx 3(n_e/10^{22})^{1/2}(B/4.414\ 10^{12})^{-1}$ keV (Ventura, Nagel, and Mészáros 1979; Soffel *et al.* 1983). Between ω_{v1} and ω_{v2} the cross sections are vacuum-dominated. The particular cross section shown is ordinary into extraordinary, there being three other graphs (not shown) *O-O*, *X-O*, *X-X*, which have matching jumps.

Photons are produced by electron-proton and electron-electron bremsstrahlung. For X-ray pulsars, at $kT < 50$ keV the latter represents only a 10% contribution (Bussard 1980; Langer, McCray, and Baan 1980), which we neglect. The cyclotron process has a much higher cross section than bremsstrahlung, but the usual expression for the cyclotron emissivity (Bekefi 1966) is inapplicable, since the assumption of LTE is not justified. For $kT \ll \hbar\omega_B$ a reasonable approximation is that of pseudo–LTE, where the cylotron absorption coefficient is replaced by the coefficient for free-freee absorption (Nagel 1980; Nagel and Ventura 1983). The expression which we use is

$$\alpha_i(\omega, \theta) = \alpha_0[\phi_+(\omega)|e^i_+|^2 g_\perp + \phi_-(\omega)|e^i_-|^2 g_\perp + \phi_z(\omega)|e^i_z|\, g_\parallel] \,, \quad (7)$$

where $g_\perp$ and $g_\parallel$ are Gaunt factors (Nagel 1980), the $e_{+,-,z}$ are the components of the ith polarization mode (Ventura 1979), and $\alpha_0 = 4\pi^2 Z^2 \alpha^3 \hbar^2 c^2 N m^{-1} \omega^{-3} (\pi m k T/2)^{-1/2}$ is the non-magnetic free-free absorption coefficient (cm^{-1}). The profile functions $\phi_{+,-,z}(\omega)$ are defined as

$$\phi_{+,-,z}(\omega) = \frac{3}{2} \frac{c}{r_0 \omega} |\,\mathrm{Im}\ T_{+,-,z}|$$

and reduce to $\phi_\pm = \omega^2/(\omega \pm \omega_B)^2$, $\phi_z = 1$ in the cold plasma limit. Equation (7) can be interpreted as giving line (cyclotron) photons via the $g_\perp$ term and continuum (bremsstrahlung) photons via the $g_\parallel$ term. The emissivity, for a one-dimensional Maxwellian distribution of electrons in the lowest Landau level, is approximated by $\epsilon_i(\omega, \theta) = \alpha_i(\omega, \theta) W(\omega)$, where $W(\omega)$ is the Wien spectrum. We neglect stimulated processes in the transfer calculation, which is why the Wien and not the Planck function is used. Similarly, equation (7) is not corrected for stimulated emission, and the detailed balance condition on the differential scattering cross section is such as to ensure that the equilibrium spectrum is of the Wien form. In Figure 2 we show the scattering cross sections, obtained by integrating equation (1) over final angles and summing over final polarizations, for various initial angles (*upper curves*). The total absorption cross sections of equation (7) are also shown in the same Figure 2 (*lower curves*). Note here the effect of the "first vacuum

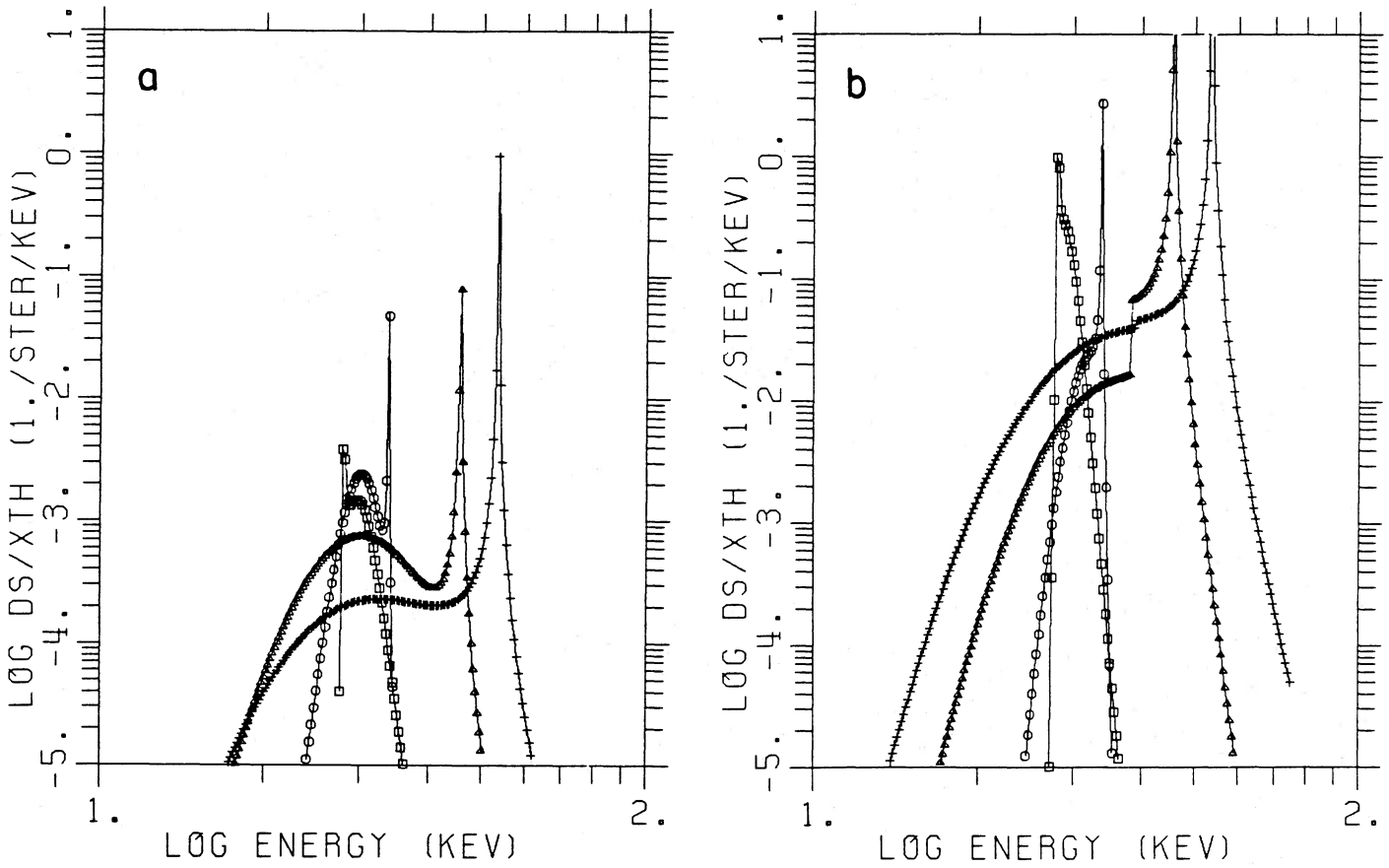

FIG. 1.—The differential scattering cross section from ordinary into extraordinary polarizations for photons of 30 keV energy in a magnetized plasma of temperature 10 keV, with cyclotron frequency at 38 keV (normalized to the Thomson value). Incoming photon angle is $\theta_i = 45°$, outgoing angles $\theta_f = 20°$, 70°, 120°, and 160° from left to right. (*a*) Without vacuum polarization; (*b*) with vacuum polarization.

frequency" ω_{v1}, near 0.4 keV. These total cross sections used $\rho = 1.67 \times 10^{-4}$ g cm^{-3}, $kT = 7$ keV, $\hbar\omega_B = 38$ keV.

III. TRANSFER EQUATION AND REDISTRIBUTION FUNCTION

In the limit of strong Faraday depolarization (Gnedin and Pavlov 1974), the Feautrier equations for slab or cylinder geometry can be written in the form (Nagel 1981*a*)

$$\left(\frac{d^2u_i}{dr^2} + \frac{\gamma}{r}\frac{du_i}{dr}\right) - K_i u_i + \sum_{j=1}^{N} S_{ij} u_j + A_i \bar{u}_i = 0 \,. \tag{8}$$

Here $u_i(\omega, \theta, r)$ is the photon density variable,

$$u_i(\omega, \theta, r) = \tfrac{1}{2}[I_i(\omega, \theta, r) + I_i(\omega, -\theta, r)] \,, \tag{9}$$

and

$$\begin{aligned} D_i(\omega_i, \theta_i) &= [(1-\gamma)\cos^2\theta_i + \gamma\tfrac{1}{2}\sin^2\theta_i]K_i^{-1}(\omega_i, \theta_i) \,, \\ A_i(\omega_i, \theta_i) &= \alpha_i(\omega_i, \theta_i) \,, \\ K_i(\omega_i, \theta_i) &= \alpha_i(\omega_i, \theta_i) + \sigma_i(\omega_i, \theta_i) \,, \end{aligned} \tag{10}$$

where $\gamma = 0$ for slab geometry, and $\gamma = 1$ for the cylinder. The α_i and σ_i are absorption and scattering coefficients (cm^{-1}), and $\bar{u}_i$ is the equilibrium (Wien) photon density. The equations (8) are obtained by taking discrete values for frequencies $\omega_k (k = 1, \ldots, K)$ and angles $\theta_l (l = 1, \ldots, L)$. As there are also two polarization modes ($m = 1, 2$), the subscript i therefore stands for the triplet (k, l, m), and the set (8) comprises $N = K \times L \times 2$ equations. The redistribution matrix S_{ij} is

$$S_{ij} = 4\pi w_{lj} \frac{d^2\Sigma_{i \leftarrow j}}{d\mu dE}(\theta_i \leftarrow \theta_j, \omega_i \leftarrow \omega_j) \,, \tag{11}$$

where the w_{lj} are weights for Gaussian quadrature in the interval [0, 1] with integration points $\cos\theta_l$. The quantity $d^2\Sigma/d\mu dE$ is the differential scattering cross section $n_e d^2\sigma/d\omega d(\cos\theta)$, evaluated over the frequency grid by means of an interpolation procedure similar to that described by Nagel (1981*b*). In that paper, scattering was assumed to occur only between the angles 60° and 120°, and it was also assumed that a photon is scattered in the forward and backward directions with equal probabilities. Here, we extend the procedure to a set of four angles instead of one. Furthermore, since the probabilities of scattering in the directions θ and $180° - \theta$ are not strictly equal, we use for $d^2\Sigma/d\mu dE$ the *average* of the forward and backward ($\pm \cos\theta_l$) probabilities. As before, the function (11) satisfies the detailed balance condition leading to a Wien equilibrium distribution. However, due to the discreteness of the angular grid, the total cross section $\sigma_i' = \sum_j S_{ji}$ is not exactly the value given by the optical theorem. As in the previous calculation, we modify the transfer coefficients, $A_i = (\sigma_i'/\sigma_i)\alpha_i$, $K_i = A_i + \sum_j S_{ji}$, $D_i = \beta_i^2/K_i$, in order to avoid purely numerical effects on the absorption probabilities and the resulting spectra.

In the present calculations we also employ the more general boundary conditions

$$\frac{\beta_i}{K_i}\frac{du_i}{dr} = -u_i + I_i^- \quad \text{at} \quad r = R\,, \tag{12a}$$

$$\frac{\beta_i}{K_i}\frac{du_i}{dr} = u_i - I_i^+ \quad \text{at} \quad r = 0\,, \tag{12b}$$

where I_i^-, I_i^+ represent the irradiation (if present) at the outer or inner surface. For slabs $\beta_i = \cos\theta_i$, and for cylinders $\beta_i = 2^{-1/2}\sin\theta_i$. Equation (12b) assumes injection in the + direction and free escape in the − direction at the inner boundary $r = 0$. An alternative interior boundary condition would be injection in the + direction and *no* escape in the − direction, which is represented by

$$\frac{\beta_i}{K_i}\frac{du_i}{dr} = -\frac{1}{2}I_i^+ \quad \text{at} \quad r = 0\,. \tag{12c}$$

Any realistic inner boundary condition must be bracketed by (12b) and (12c). If radiation is incident neither from below nor from above (self-emitting slab), then due to symmetry it is sufficient to perform the calculation for half a slab, and the inner boundary condition (12b) can be replaced by

$$\frac{du_i}{dr} = 0 \quad \text{at} \quad r = 0 \tag{12d}$$

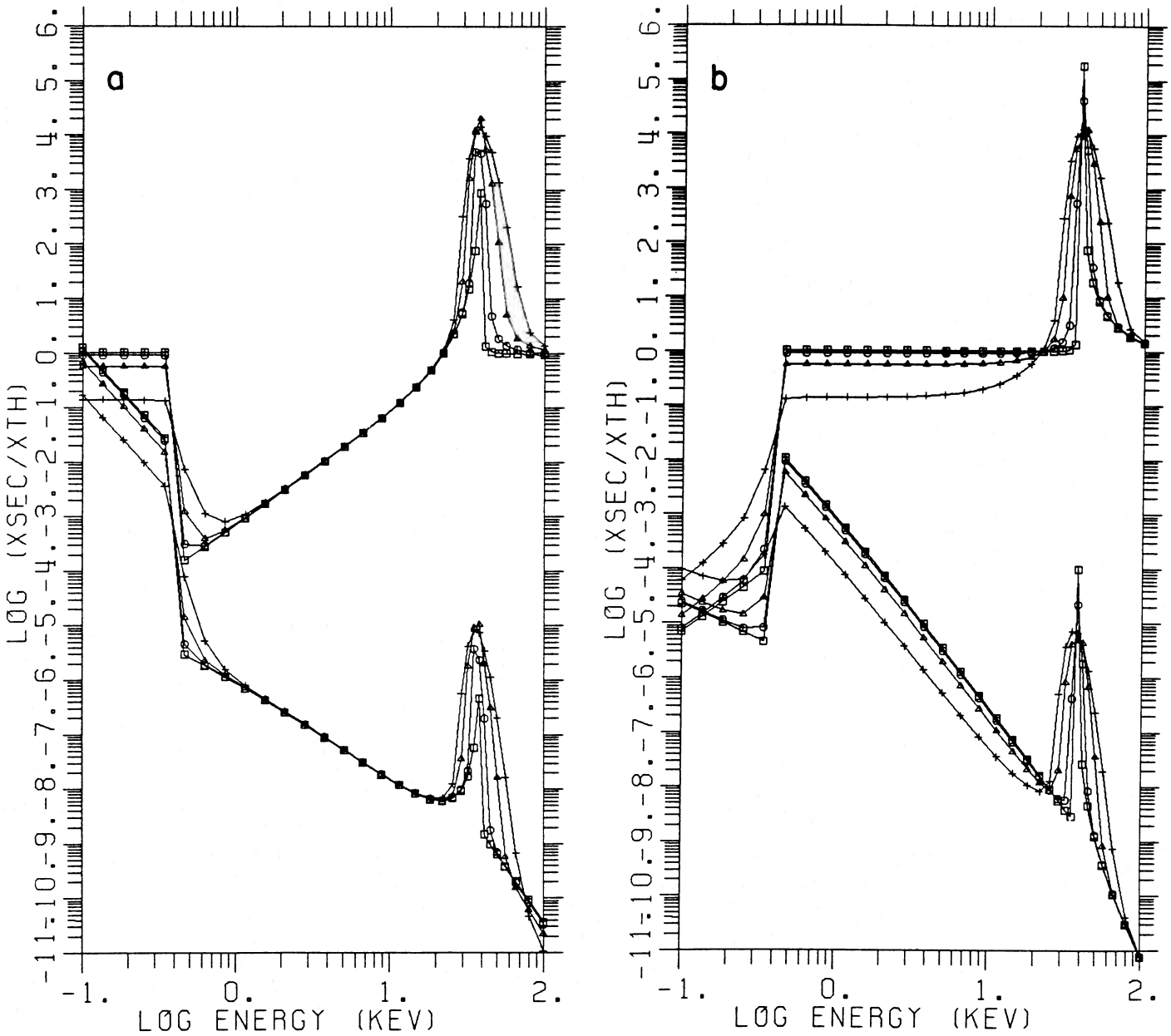

FIG. 2.—The total scattering cross section σ_i and total absorption cross sections α_i, normalized to the Thomson value, are shown for angles $\theta = 21°$, 48°, 71°, and 86° (crosses, triangles, circles, and squares respectively). Vacuum polarization is included, with $\rho = 1.67 \times 10^{-4}$ g cm^{-3}, $kT = 7$ keV, and $\omega_B = 38$ keV. The upper curves are scattering, the lower ones absorption. The polarization is (*a*) ordinary, (*b*) extraordinary.

(where now $r = 0$ corresponds to the middle of the slab, not its lower boundary), and the lower boundary at $r = -R$ is free. If the lower boundary is *not* free (i.e., it is perfectly reflecting) then condition (12d) is still valid bur $r = 0$ is not the middle of the slab but the actual inner boundary.

IV. RESULTS

a) Case A: Self-emitting Atmospheres

Computations were carried out with a set of 32 frequencies, four angles, and two polarizations, for both slabs and cylinders. The magnetic field direction was taken to be perpendicular to the surface of the slab, and parallel to the axis of the cylinder. The magnitude of B was 3.3×10^{12} G, or $\hbar\omega_B = 38$ keV, the density $\rho = 0.5$ g cm^{-3}, and the temperature $kT = 8$ keV. The depth of the slab or column was chosen as $y = 50$ g cm^{-2}. In the case of the slab such a depth is characteristic of the stopping length of protons via Coulomb and nuclear collisions (e.g., Mészáros *et al.* 1983). We considered here only thermal emission in the slab or column itself, using the boundary conditions (12a) and (12d) with $I_i^- = 0$ (no incident radiation from above), so that with a polar cap of an area ~ 10 km^2 one obtains a luminosity of $\sim 10^{37}$ ergs. Figures 3*a* and 3*b* show the angle-integrated flux per unit area (photons s^{-1} cm^{-2} keV^{-1}) from a slab and a column respectively. The differential fluxes $I_\omega(\theta)\cos\theta$ or $I_\omega(\theta)\sin\theta$ (photons s^{-1} cm^{-2} keV^{-1} sr^{-1}) for the same configurations are shown in Figures 3*c* and 3*d*. The four angles are $\theta = 21°$, 48°, 71°, and 86°. In the slab, the differential flux tends to decrease with the angle θ, whereas for the column it tends to increase. This is just a consequence of the usual limb darkening effect.

Between 5 and 20 keV the average spectral indices of slab and column are close to zero, the spectrum of the column being slightly steeper. This happens to agree with the usual finding for nonmagnetic Comptonization (Sunyaev and Titarchuk 1980) that media of large Thomson depth lead to flat spectra (saturated Comptonization). It should be noted, however, that the strong frequency dependence of the photon-scattering cross sections in a magnetic field make such comparisons difficult.

As expected for this optical depth, the cyclotron line appears in absorption, and the width increases for angles close to the field direction. One has roughly

$$\Delta\omega_{\rm FWHM} \approx \omega_B \left(8 \ln 2 \frac{kT}{mc^2} \right)^{1/2} \cos\theta , \qquad (13)$$

i.e., the line gets broader as one looks along the direction of motion of the electrons. The resonance frequency, determined by the zero of the denominator of the Π_- matrix element, is approximately

$$\omega \approx \omega_B + p\frac{\omega\cos\theta}{mc} + \frac{\hbar\omega^2\cos^2\theta}{2mc^2} . \qquad (14)$$

The first correction is either positive or negative, depending on the direction of motion of the electron, but the second-order correction $\omega^2\cos^2\theta/2m > 0$ shows that the angles close to 0° give a higher resonant frequency than the angles close to 90°. This effect is seen in the position of the dip in Figures 3*c* and 3*d*. This occurs for both slab and column geometry. On the other hand, the flux depends on the angle with respect to B differently for slab ($I\cos\theta$) and column ($I\sin\theta$) geometry, as indicated before. The combination of these two effects therefore produces a small correlation of the line energy with the continuum intensity in the slab case and an anticorrelation of these quantities in the case of a radiating column.

The position of the peak on the high-energy side of the line depends on angle more strongly than does the position of the dip. It is at this peak (the "blue shoulder" of the line) where the absorption line joins the steep continuum. As the line becomes very broad at small angles ($\Delta\omega \propto \cos\theta$), the blue shoulder moves to higher and higher energies. This is indicated by Figures 3*c* and 3*d*, especially by the curves for 48° and 71°. Unfortunately, in these figures the line is not resolved at large angles (86°), and at small angles (21°) the line shown is too shallow, due to the neglect of spin-flip transitions. The line is better resolved at low optical depths, cf. §§ IV*b* and IV*c*. The behavior described above is more clearly visible in Figure 3*e*, showing results of a calculation (Nagel, unpublished) on a simplified model for a semi-infinite atmosphere with the magnetic field perpendicular to the surface, and assuming complete redistribution in the cyclotron line. Although the model is rather crude (the cyclotron absorption cross section is approximated by a simple Gaussian, and polarization effects are ignored), it is reassuring that the results are in qualitative agreement with those obtained by the Feautrier method.

b) Case B: External Irradiation at the Outer Boundary

The frequency and angle grid was again set at 32×4, with $\hbar\omega_B = 38$ keV. The density was taken to be $\rho = 1.67 \times 10^{-4}$ g cm^{-3} ($n_e = 10^{20}$ cm^{-3}), characteristic of free fall on to a neutron star, with adiabatic compression behind a shock, assuming $\dot{M} = 10^{17}$ g s^{-1}. The total depth of the atmosphere was assumed to be $R = 1$ km, and the temperature $kT = 7$ keV, in order to obtain a typical continuum spectrum. At such low densities the thermal emission in the slab (or column) is insufficient to produce a luminosity comparable to the observed luminosity $L_x \approx (GM/R_*)\dot{M} \approx 10^{37}$ ergs s^{-1}. However, the observation of a very soft ($E < 1$ keV) component in some pulsars such as Her X-1 and SMC X-1 (e.g., Holt and McCray 1982) suggests the possibility of an extraneous source of soft photons. These soft photons could come from the Alfvén surface or from the disk, if thermal, or from a smaller region near the surface or in the column, if nonthermal. We assume here that the slabs or columns are illuminated with radiation $I_{\rm ext}^-$ having a blackbody spectrum corresponding to a temperature $T_{bb} = 0.1$ keV, but an intensity per unit area 10^4 times higher than the blackbody intensity corresponding to 0.1 keV. This is suggested by the observed values of $L_{\rm soft}$ of order 10% of the hard luminosity, or $L_{\rm soft} \approx 10^{36}$ ergs s^{-1}. We assume this amount of soft energy to be incident on the *outer* boundary of the slab or cylinder, whose outside surface is again of order 10 km^2. The boundary conditions used are (12a) and (12d), with $I_{\rm ext}^- \neq 0$. In addition, there is of course the emission and absorption in the atmosphere itself.

The results for these parameters, and external illumination from the outside are shown in Figures 4*a* and 4*b* (angle-integrated flux for slab and column) and 4*c* and 4*d* (differential flux in these two cases). A significant fraction of the soft photons are up-Comptonized by the hot atmosphere, through which they have to diffuse before they can escape. This leads to a power-law spectrum at $E_s \ll \hbar\omega < kT$, with an exponential roll-over at $\hbar\omega \approx 3kT$, and of course the cyclotron feature at $\hbar\omega_B = 38$ keV. The average 2–20 keV slope of the slab (Fig. 4*a*) is near -1, similar to the "typical" value observed in, e.g., Her X-1. The slope for the column of the same optical

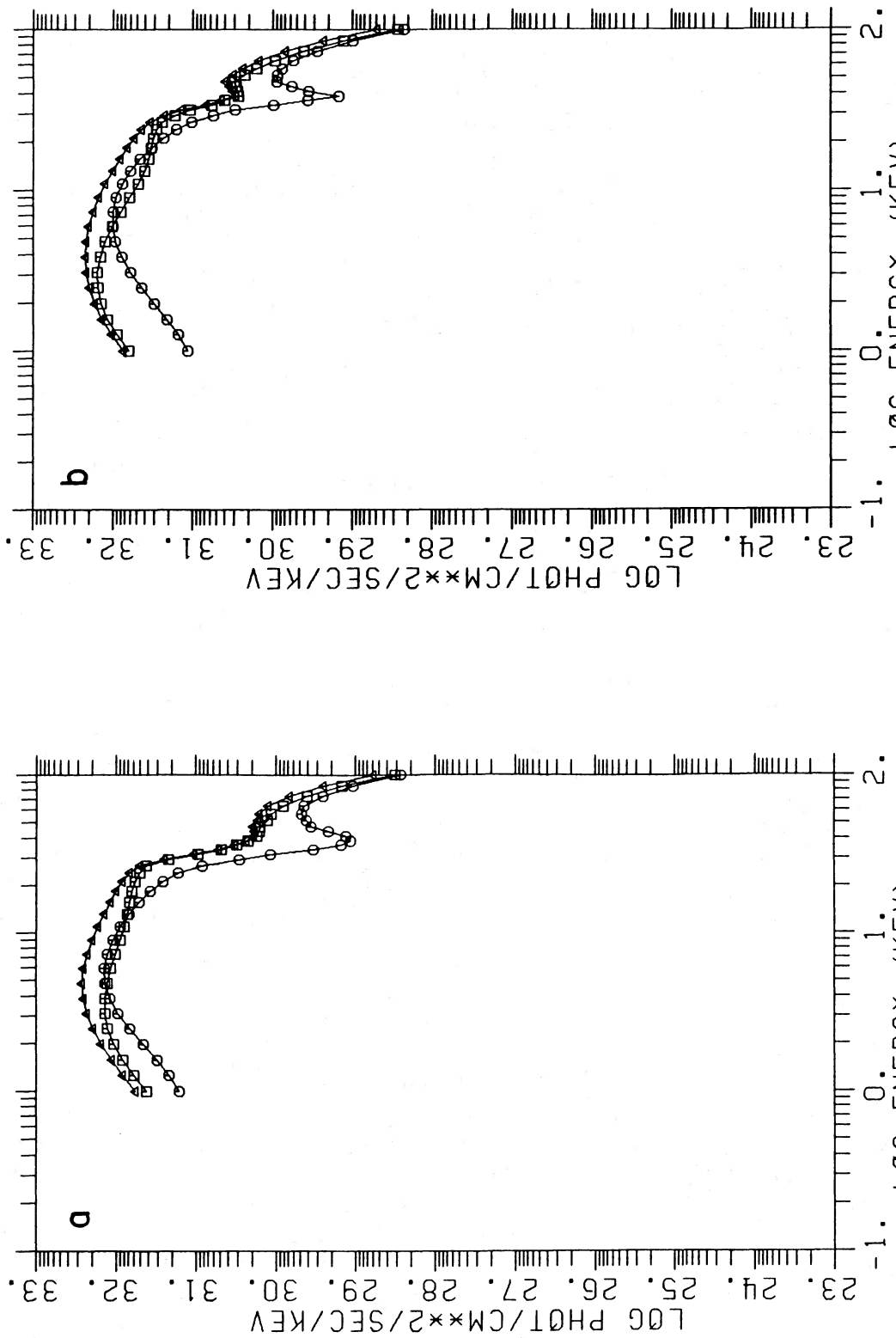

FIG. 3.—Spectra of self-radiating atmosphere with $\hbar\omega_B = 38$ keV, $kT = 8$ keV, $\rho = 0.5$ g cm^{-3}. Symbols are *square*, ordinary; *circle*, extraordinary; *triangle*, total flux. (*a*) Slab (thickness $R = 100$ cm); (*b*) column (radius $R = 100$ cm).

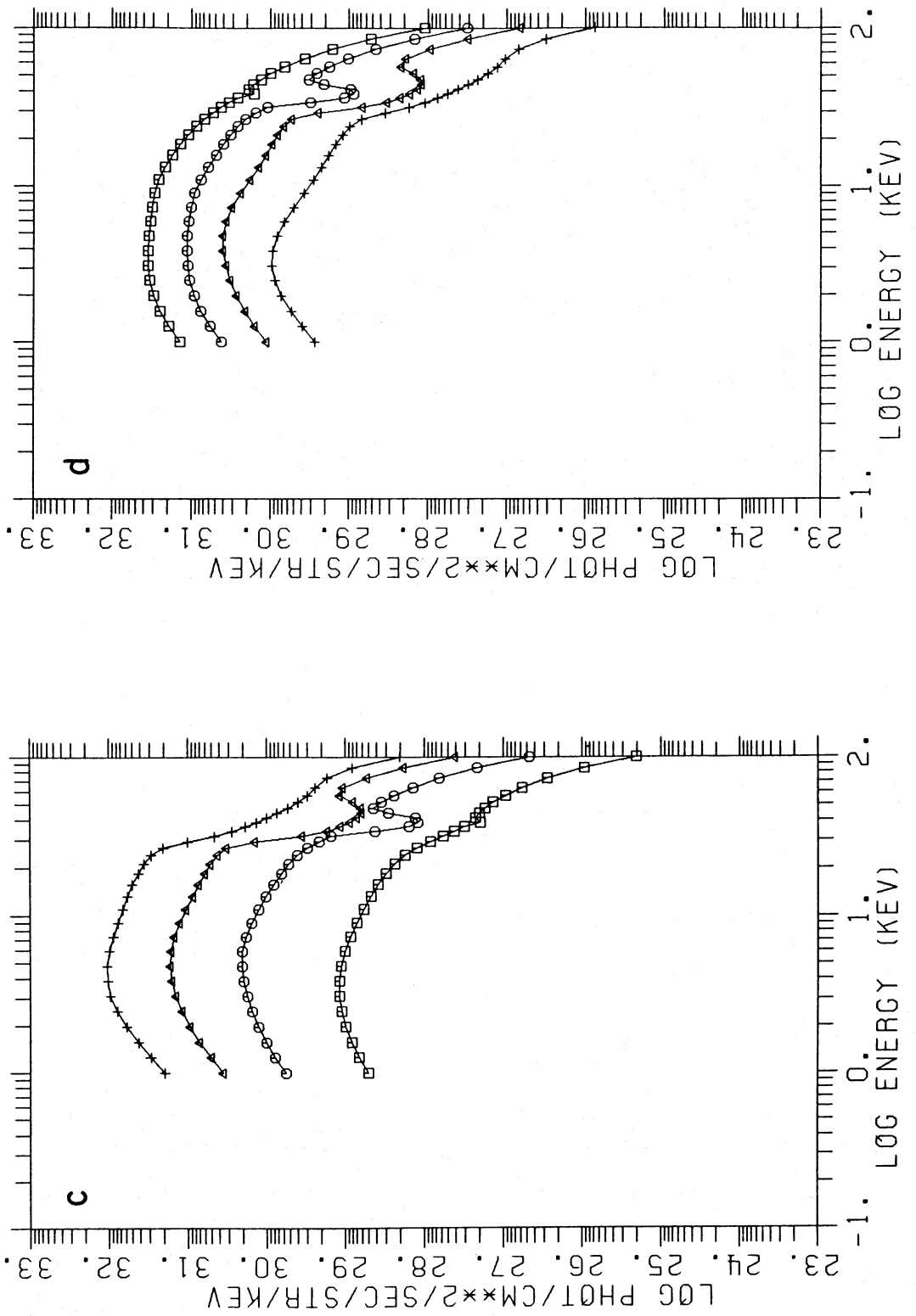

FIG. 3.—(*c*) Slab spectra (total) emerging in directions $\theta = 21°, 48°, 71°$, and 86° (*cross, triangle, circle, square*); (*d*) column spectra (total), similarly

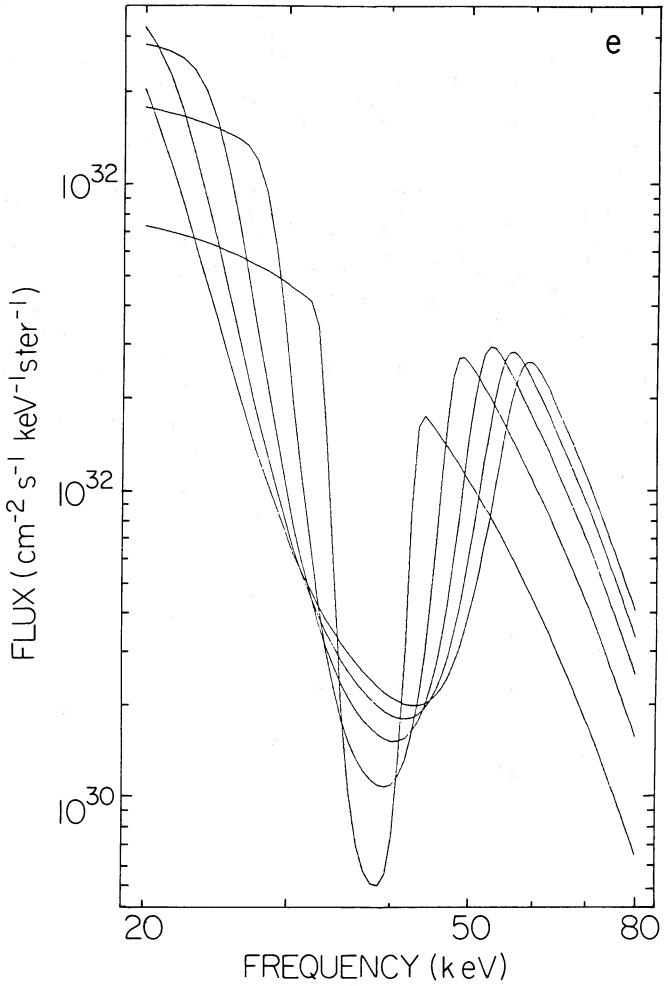

FIG. 3*e*.—Slab spectra (total) computed under the assumption of complete redistribution in the cyclotron line, with a Gaussian line shape. The thickness of the slab is essentially infinite. The escaping flux $I_\omega(\theta)\cos\theta$ is shown for the directions $\theta = 0°, 30°, 45°, 60°$, and 75°.

depth (Fig. 4*b*) is slightly steeper, a result which is to be expected, since from a column photons can escape more easily than from a slab. The differential fluxes $I_\omega(\theta)\cos\theta$ (slab) and $I_\omega(\theta)\sin\theta$ (column) are shown in Figures 4*c* and 4*d*. The structure of the line is very similar. It appears again as an absorption line, and the previously discussed correlation between the line energy and neighboring continuum intensity is also seen here. However, the line is much more noticeable than in the previous self-emitting case of Figure 3. This can be explained by the lower ratio of line to continuum photon *creation* in Figure 4, where the photons are mostly upscattered soft ones, which then are scattered out of the line. In Figure 3, on the other hand, photons are thermally created, and more of them are created near ω_B. Even though photons are being scattered out of the line in Figure 3, they are also being created at a fast rate, and the depression near ω_B is less deep.

It is instructive to compare these calculations using four angles with the previous method (Nagel 1981*b*), which used only one "typical" direction, $\theta = 60°$. The spectra obtained with four angles are significantly steeper, i.e., less Comptonized. This is easy to understand from the properties of the scattering cross section in strongly magnetized plasma (cf. Fig. 2). For directions nearly parallel to the magnetic field, the opacities are strongly reduced at low frequencies. Thus in the four-angle computations the 21° channel provides a leak through which low-energy photons can escape before they reach high energies. The effective thickness of the medium is then reduced. This effect does not increase significantly by going to eight angles. Note, however, that the spectrum at high energies is only weakly affected when Comptonization is saturated (e.g., for self-emitting thick slabs).

c) Case C: External Irradiation at the Inner Boundary

The case of external irradiation incident in the + direction at the inner boundary, with no escape in the − direction at the inner, and free escape at the outer boundary, is obtained using the boundary conditions (12a) and (12c) with $I^+_{\rm ext} \neq 0$, $I^-_{\rm ext} = 0$. For the slab, this represents a photon source at the stellar surface. For the cylinder, this is more artificial, being a line source at $r = 0$, which may roughly correspond to photons from a central surface mound, initially directed upward and scattered sideways. We took again $kT = 7$ keV, $\rho = 1.67 \times 10^{-4}$ g cm^{-3}, $R = 10^5$ cm, $\hbar\omega_B = 38$ keV, and the same blackbody spectrum and intensity enhancement factor as before. The spectra are very similar to the previous case. The total flux resulting from reflection (case B) and transmission (case C), with no escape from the lower boundary, is plotted in Figure 5 for the slab geometry. The triangles are B, circles are C, these being the top two curves between 2 and 20 keV, very close to each other. The soft flux seen in C is that *transmitted* from the atmosphere, while in the previous case (B) it was reflected, the latter being slightly larger. The hard X-ray flux, made of up-Comptonized photons escaping from the top of the atmosphere, is very similar in both B and C. The spectrum between 2 and 10 keV has an energy spectral index $\alpha \approx {}^{-1.0}_{-0.8}$, close to representative values for X-ray pulsars. The correlation between line energy and continuum intensity is present in this case as well.

In the hard X-rays the reflected and transmitted spectra, for a slab of a given size, are almost identical. This is similar to the nonmagnetic case (see, e.g., Sunyaev and Titarchuk 1980), and is easily understood as a consequence of the fact that photons which have stayed in the slab for a long enough time to reach high energies have "forgotten" from which side they were injected.

d) Cases D, E, and F: External Illumination with Free Escape at Both Boundaries

In cases B and C it was assumed that at the inner boundary, $r = 0$, no radiation escape was allowed in the − direction. Alternatively, we may assume *free* escape in the − direction at $r = 0$, while keeping the condition of free escape in the + direction at $r = R$ unchanged, as in cases B, and C. Thus for the inner boundary we may use condition (12b) and for the outer one (12a). Clearly, for the same optical depth and external illumination one expects less Comptonization than in the previous cases B and C, since now photons can escape from *both* boundaries, rather than just from the outer one. This is indeed borne out by the calculations, for which we used again the same ρ, T, B, and R as in B and C, for slabs only. In Figure 5 we show the total (polarization summed) slab flux of the reflection case D with plusses, and of transmission case E

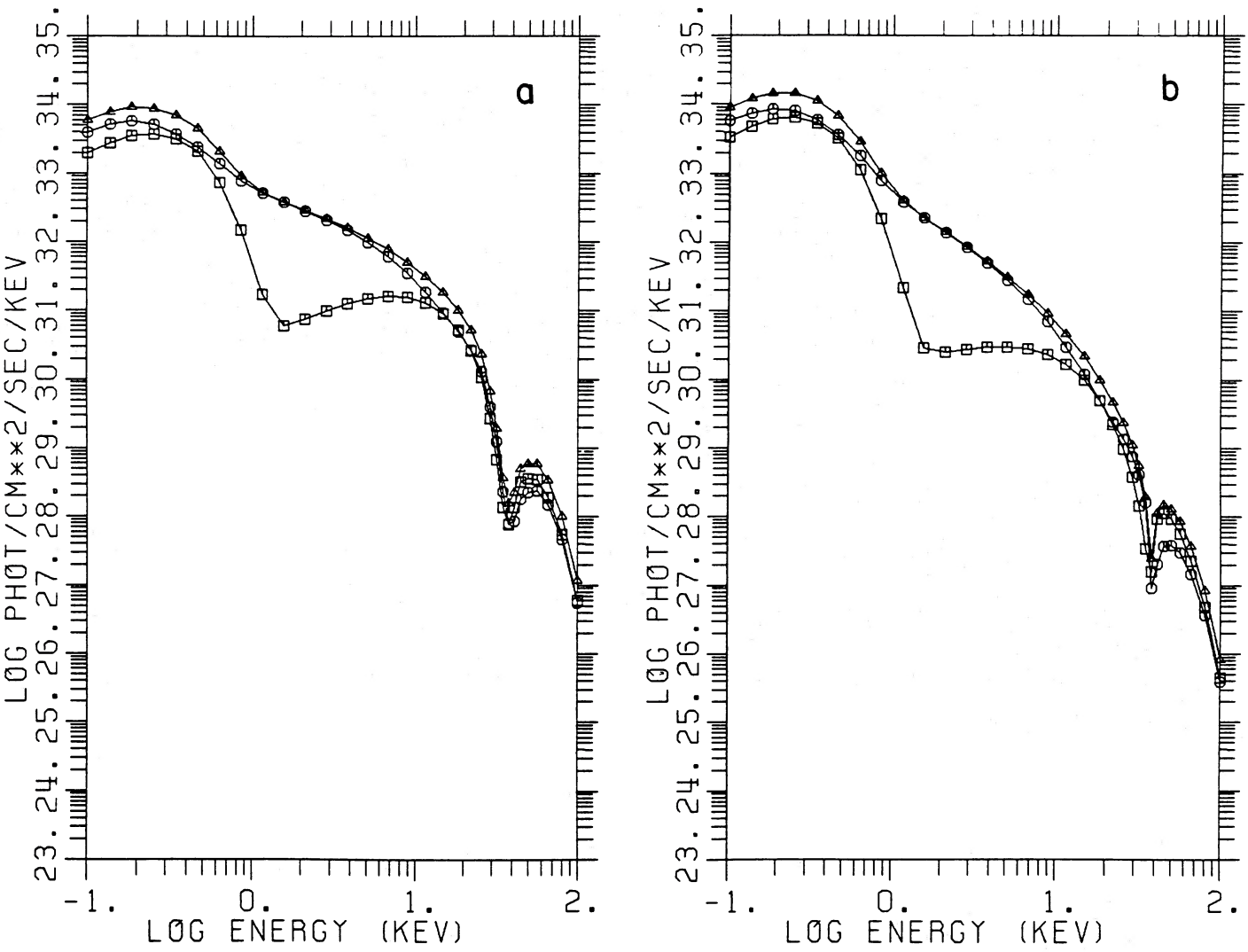

FIG. 4.—Spectrum of an externally illuminated atmosphere (reflection), $\hbar\omega_B = 38$ keV, $kT = 7$ keV, $\rho = 1.67 \times 10^{-4}$ g cm^{-3}. The square, circle, triangle and cross have the same interpretation as in the corresponding Fig. 3*a–d*. (*a*) Slab (thickness $R = 10^5$ cm); (*b*) column (radius $R = 10^5$ cm).

with crosses. These are the two lowest curves between 2 and 100 keV, coincident to the point that the straight and diagonal crosses are confused into a single asterisk-like symbol. However, below 2 keV, the soft transmitted and reflected fluxes are different. The 2–20 keV slope is now ~ -1.8, rather steeper than typical values. However, if we keep the same boundary conditions and ρ, T, B, but increase R by twice (to $R = 2 \times 10^5$ cm), case F, we obtain the curve marked by squares, which is very similar to the slab cases B and C, shown as circles and triangles respectively. In particular, the slope of ~ -1 is again obtained.

V. DISCUSSION

The models considered are necessarily very idealized. As in previous calculations, we have taken the accretion column to be homogeneous and neglected bulk motions. However, the present calculations provide new information on the pulse phase dependence of the spectrum, because we calculated the simultaneous angle and frequency redistribution. The introduction of more general boundary conditions has also made it possible to investigate the effects of external photon sources.

The inclusion of vacuum polarization effects, which modifies the cross sections significantly (Figs. 1 and 2), has a strong influence on the polarization of the emergent radiation. It is responsible for the crossover of the ordinary and extraordinary flux seen around 3 keV in Figure 3, and it also contributes to the depth of the resonance feature at 38 keV. The polarization-summed flux around 3 keV does not show an effect, because the partial fluxes tend to compensate each other. Self-emitting homogeneous atmospheres of lower optical depths than used here, however, appear more capable of showing an effect near this vacuum frequency in the total flux.

The cyclotron line, as already indicated by Nagel (1981*b*), appears in absorption, because photons are scattered out of the resonance. The energy of the trough is weakly dependent on the angle θ. A stronger variation with angle is shown by the peak of the blue shoulder of the line, see Figures 3 and 4. We

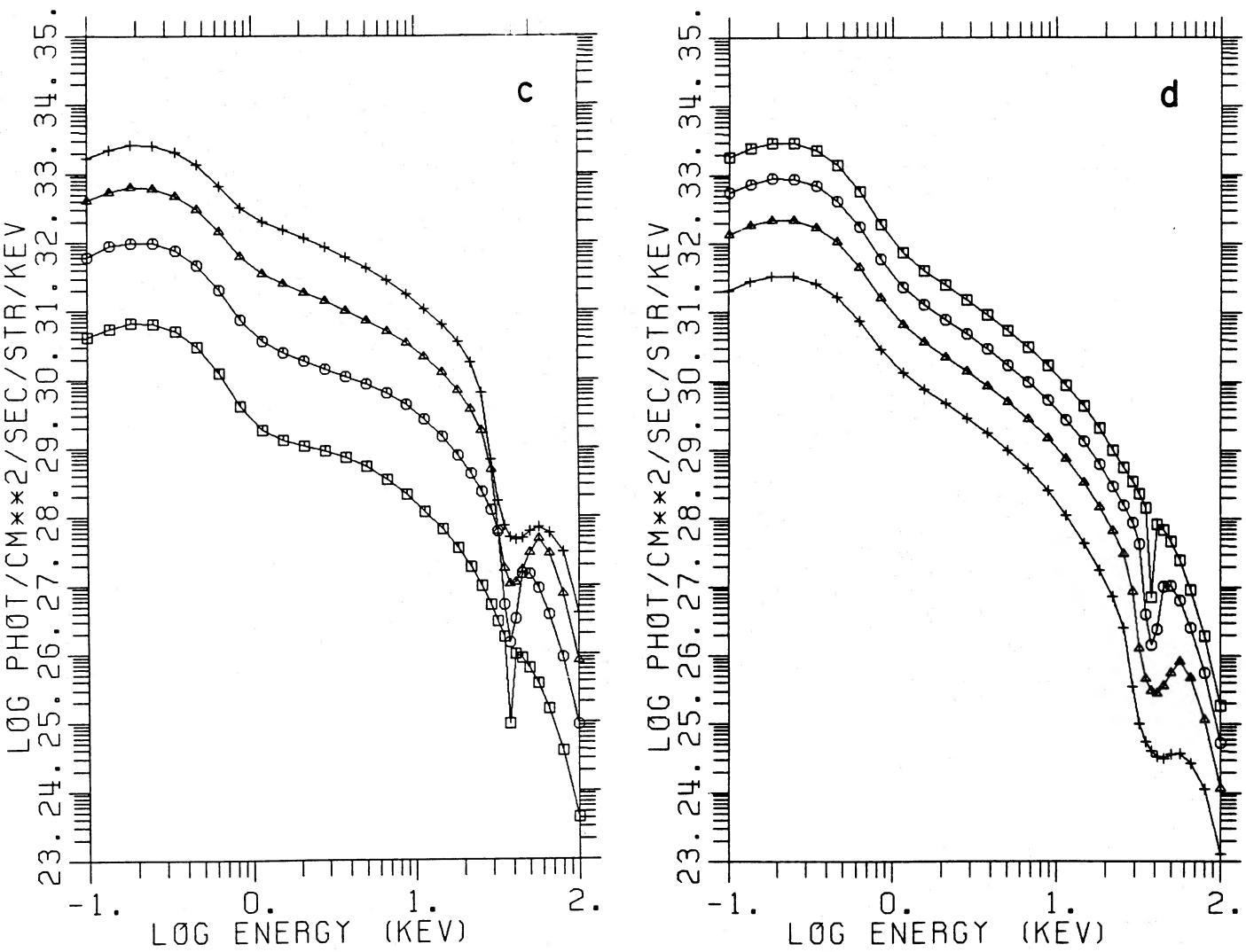

FIG. 4.—(*c*) Slab spectra emerging in directions $\theta = 21°, 48°, 71°$, and 86°; (*d*) column spectra emerging in directions $\theta = 21°, 48°, 71°$, and 86°

have plotted in Figure 6*a* the blue-shoulder peak energy as a function of θ for the two slab models of Figures 3 and 4, complemented by further eight-angle Feautrier calculations. To convert these to a phase ϕ we use the expression

$$\cos\theta = \cos i_1 \cos i_2 + \sin i_1 \sin i_2 \cos[2\pi(\phi - \phi_0)] , \quad (15)$$

where i_1 is the angle between the line of sight and the rotation axis of the neutron star, and i_2 is the angle between the rotation axis and the magnetic axis.

For a pencil beam (slab model), the angles closest to $\theta = 0$ correspond to phase $\phi = 0$. For a fan beam (column model), the behavior is opposite, and at phase $\phi = 0$ the angle θ is closer to 90°, with the interpretation in both cases that the intensity is maximum (main pulse) at $\phi = 0$. When equation (15) yields $\theta > 90°$, the other magnetic pole is visible, and we replace θ by $180° - \theta$, assuming the poles to be symmetric. We show in Figures 6*b* and 6*c* the energy of the blue-shoulder peak for the slab models as interpolated or extrapolated from Figure 6*a*, taking viewing angles $(i_1, i_2) = 60°/45°$ and 45°/45°. (Note that eq. [15] is symmetric in i_1 and i_2). For the slab models, the blue wing peaks at the highest energy for $\phi = 0$. If the viewing angles are such that the second pole is not sampled (e.g., 45°/45°), then the minimum blue wing energy occurs at $\phi = 0.5$. In the other case, if the other pole is also seen (producing an interpulse), the energy of the blue wing is minimum shortly before phase 0.5, and then it increases again to reach a secondary maximum at phase $\phi = 0.5$, with the primary maximum still at $\phi = 0$. We may compare these results with the compilation by Voges *et al.* (1982) of the MPE/AIT balloon and MIT/UCSD *HEAO 1* data on Her X-1, which gives the phase dependence of an assumed emission-line centroid, shown in Figure 6*d*. This comparison should be made with some caution, since the spectra plotted in Figure 6*d* were deconvolved from the count spectra using an *emission* line model. What we show in Figures 6*b* and 6*c* is, on the other hand, the peak on the blue wing of the absorption line obtained in our models. The similarity is encouraging between both (arbitrarily chosen) viewing angles 60°/45° and 45°/45° and the data of Figure 6*d*. If one uniformly "redshifts" our calculated centroids by about 15%, then the agreement between Figures 6*b*, 6*c*, and 6*d* becomes quite good. Two effects not included in the present calculation that could force the blue shoulder to slight-

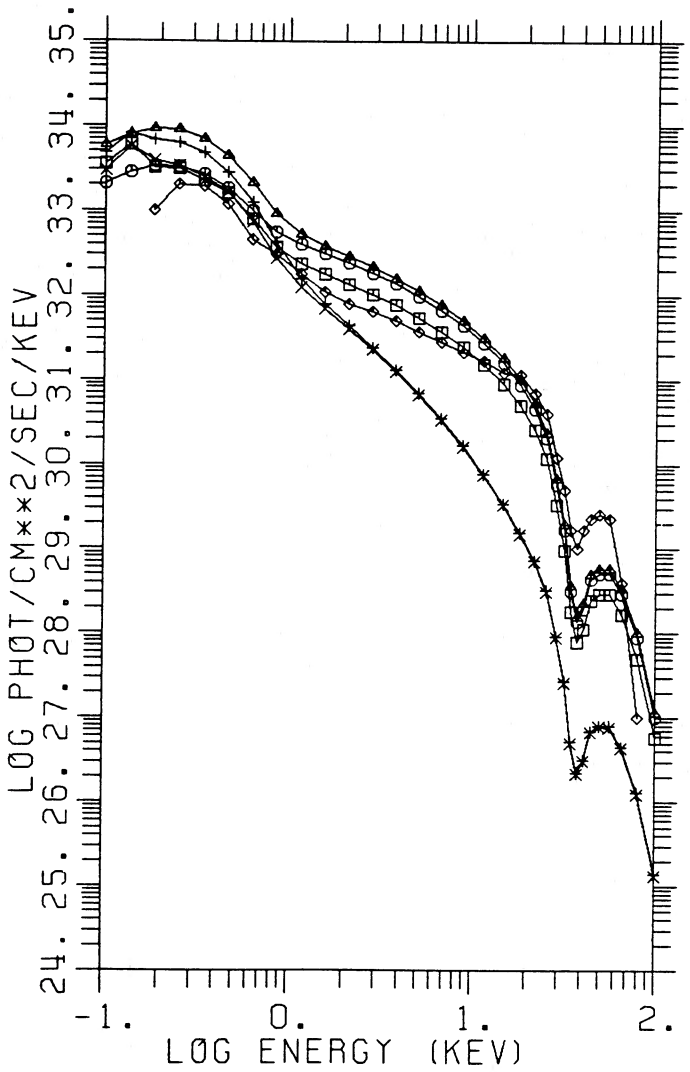

FIG. 5.—Total flux from various externally illuminated slab models, compared to a composite observed spectrum of Her X-1, taken from Holt and McCray (1982). The various symbols are, reading along 2–10 keV from top to bottom *triangles*, model B (Fig. 4*a*), externally illuminated (outer), no escape (inner), $R = 10^5$ cm. *circles*, model C, externally illuminated (inner), no escape (inner), $R = 10^5$. *squares*, model F, externally illuminated (inner), free escape (inner), $R = 2 \times 10^5$. *diamonds*, data for Her X-1. *plusses*, model D, externally illuminated (outer), free escape (inner), $R = 10^5$. *crosses*, model E, externally illuminated (inner), free escape (inner), $R = 10^5$.

ly lower energies are the inclusion of a first harmonic, e.g., Mészáros, Nagel, and Bussard (1984), and a non-Maxwellian distribution with deficiency of electrons at $E > \hbar\omega_B$, e.g., Langer, McCray, and Baan (1980). In general, it appears that the slab models may be made to fit data of the kind shown in Figure 6*d*, whereas column models may not. From Figures 3 and 4 we see that the trend for columns would be opposite to the slab case: low energy of the spectral peak at high flux (phase 0), and high energy at low flux (phase 0.5). This analysis indicates that models with pulse maximum (phase 0) occurring when the field is pointing closest to us are observationally favored.

The angle-integrated spectra of Figures 3*a* and 3*b*, 4*a* and 4*b*, and 5 may also be compared with the phase-averaged spectra of different X-ray pulsars. White *et al.* find an average (energy) spectral index of 0.4 for a sample of 12 X-ray pulsars, with two being close to -0.5, and four being close to 0.3, ..., 0.5. As explained in the previous section, the parameters of our self-emitting atmospheres can be adjusted to give the required spectral index in the hard X-ray regime. Below about 5 keV the spectra of the self-emitting atmosphere turn over toward the Wien spectrum, as expected, since we neglected stimulated scattering. In reality the limiting spectrum is the Planck function, which is less steep, so that the low-energy turnover would occur at somewhat lower energies. However, a single (flat) power law all the way down to 1 keV seems difficult to reproduce in the self-emitting model, and even less a soft (<1 keV) excess or hump—unless we introduce some other component or element into the picture.

This motivated us to explore the effect of "external" photon sources in §§ III*b*, III*c*, and III*d*. The other consideration leading to this type of model is that the particle density, either in free fall or just below a stand-off shock, would have to be much lower than assumed in our self-emitting atmosphere models ($n_e \lesssim 10^{20}$ cm^{-3}). Such rarefied plasmas do not produce enough thermal photons to explain the observed luminosity $L_x \approx 10^{37}$ ergs s^{-1}. If there is, however, near or inside the column a strong source of nonthermal soft photons (such as might also explain the observed soft excess of some X-ray pulsars), then these soft photons would also be partially Comptonized in the accretion column and produce a power-law spectrum between $\hbar\omega_{\rm soft}$ and kT. In this case, the luminosity in hard X-rays is due to the thermal (accretion) energy of the electrons, but the seed photons are provided by the soft source. It should be stressed that for this to work the flux of soft photons incident on the boundary of the hot atmosphere (area ~ 10 km^2) has to be suprathermal relative to their color temperature ($kT_{\rm color} \approx 0.1$ keV). The enhancement factor (above blackbody) which we used was 10^4, and we have not made any attempt here at justifying this source of soft photons (see, however, Bussard, Mészáros and Alexander 1985). The angle-averaged photon spectra of such slab or column atmospheres were shown in Figures 3, 4, and 5.

These spectra may be compared to a phase-averaged spectrum of, e.g., Her X-1 (Holt and McCray 1982), which we have included in Figure 5 with the diamond symbol. The slab spectra of cases B and C with $R = 10^5$ cm and of D with $R = 2 \times 10^5$ cm look qualitatively similar to the observations. This by itself cannot be considered an argument against the cylinder geometry (in this source), since modest increases in either the density or the depth could flatten the slope to the required value. It does, however, provide some supporting evidence for the slab geometry, when combined with the shift of the blue wing peak with phase (as discussed above).

We have not attempted to explain with our simplified model the effect observed in Her X-1 of an increase in soft ($E < 1$ keV) flux, which is $\sim 180°$ out of phase with the hard X-ray pulses (e.g., Holt and McCray 1982). To explain this feature, one would have to consider in more detail the origin of the soft photons. Similarly, we have not addressed the question of the Comptonization caused by the velocity shear in a radiation shock (see Lyubarski and Sunyaev 1982), since we have neglected bulk motions. This is one of the simplifications which allows us to treat the magnetic field effects on the radiative transfer in reasonable detail.

Even considering all the simplifications introduced, one conclusion that we believe will persist in more sophisticated calculations is that the observations seem to be more easily

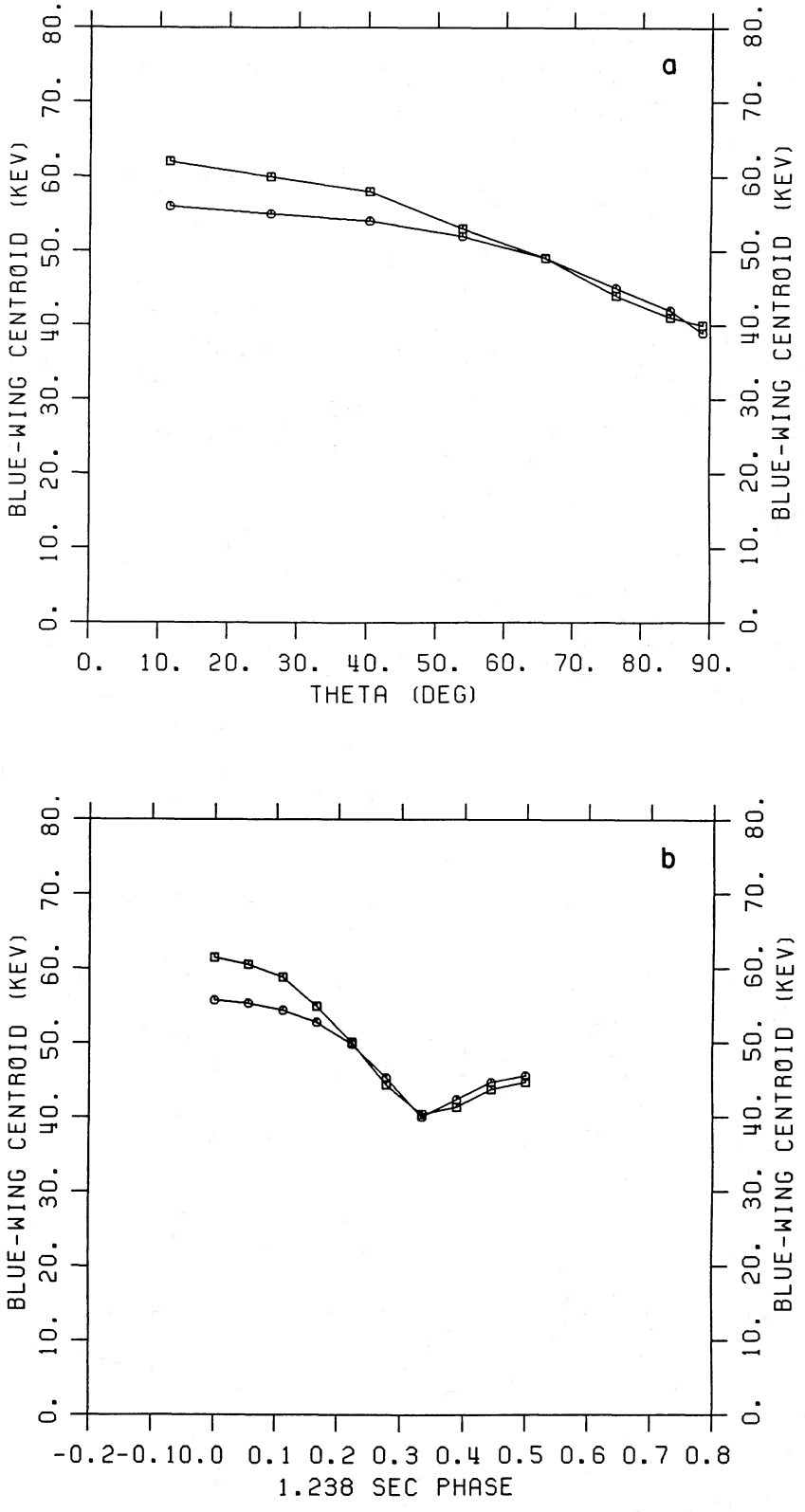

FIG. 6.—(*a*) Position of the blue wing peak in the spectra as a function of angle, for the slab models of Fig. 3 (*circles*) and Fig. 4 (*squares*). (*b*) Shift of the blue wing peak with pulse phase, as derived from the data of Fig. 5, using the angles $(i_1, i_2) = (60°/45°)$. (*c*) Same for (45°/45°). (*d*) Observed points from *HEAO 1*, 1978 February (*plusses*) and MPI/AIT, 1977 September (*circles with plusses*), from Voges *et al.* 1982).

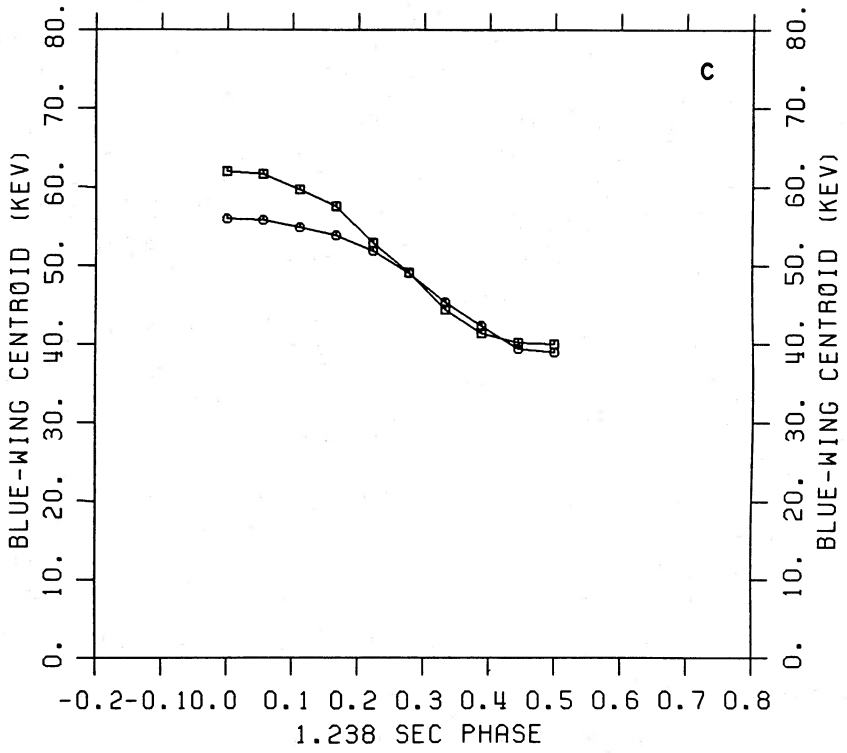

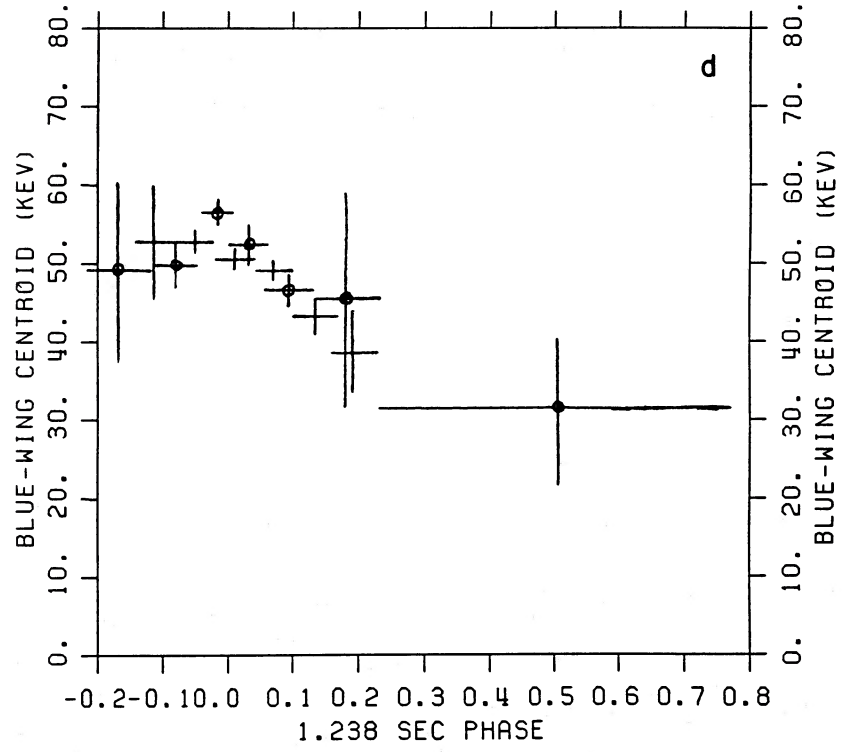

FIG. 6—*continued*

explained with the slab mode. In the case of Her X-1, this has already been suggested by Nagel (1981*a*), and by White, Swank, and Holt (1983) for the high-luminosity objects. This may seem somewhat surprising, since in luminous sources such as Her X-1 one might expect a radiation deceleration shock, whose standoff distance could be a fraction of the stellar radius (Wang and Frank 1981), suggesting column geometry. However, the radiation hydrodynamics problem in the strong magnetic field is as yet unsolved. If the standoff distance were smaller than the polar cap radius, a pencil beam would be plausible, and the present calculations may be indicating that this is the case.

This research has been partially supported through NSF grant AST 83-13886. Access to supercomputer time was provided by the Max Planck Institute, Munich, and by the NSF.

REFERENCES

Bekefi, G. 1966, *Radiation Processes in Plasma* (New York: Wiley).
Bonazzola, S., Heyvaerts, J., and Puget, J. L. 1979, *Astr. Ap.*, **78**, 53.
Bussard, R. W. 1980, *Ap. J.*, **237**, 970.
Bussard, R. W., Mészáros, P., and Alexander, S., 1985, *Ap. J. (Letters)*, **297**, L21.
Canuto, V., Lodenquai, J., and Ruderman, M. 1971, *Phys. Rev. D*, **3**, 2303.
Gnedin, Yu. N., and Pavlov, G. G. 1974, *Soviet Phys.—JETP*, **38**, 903.
Gnedin, Yu. N., Pavlov, G. G., and Shibanov, Yu. A. 1978, *Soviet Phys.—JETP (Letters)*, **27**, 305.
Harding, A. K., Mészáros, P., Kirk, J. G., and Galloway, D. J. 1984, *Ap. J.*, **278**, 369.
Holt, S. S., and McCray, R. 1982, *Ann. Rev. Astr. Ap.*, **20**, 323.
Kaminker, A. D., Pavlov, G. G., and Shibanov, Yu. A. 1982, *Ap. Space Sci.*, **86**, 249.
Kanno, S. 1980, *Pub. Astr. Soc. Japan*, **32**, 105.
Kirk, J. G. 1980, *Plasma Phys.*, **22**, 639.
Kirk, J. G., and Mészáros, P. 1980, *Ap. J.*, **241**, 1153.
Langer, S. H., McCray, R., and Baan, W. 1980, *Ap. J.*, **238**, 731.
Lyubarski, Yu. E., and Sunyaev, R. A. 1982, *Soviet Astr. Letters*, **8**, 330.
Mészáros, P., and Bonazzola, S. 1981, *Ap. J.*, **251**, 695.
Mészáros, P., Harding, A. K., Kirk, J. G., and Galloway, D. J. 1983, *Ap. J. (Letters)*, **266**, L33.
Mészáros, P., Nagel, W., and Bussard, R. W., 1984, in *X-Ray Astronomy 84*, ed. M. Oda and R. Giacconi, Tokyo: Institute of Space and Astronautical Studies), p. 181.
Mészáros, P., Nagel, W., and Ventura, J. 1980, *Ap. J.*, **238**, 1066.
Mészáros, P., and Ventura, J. 1978, *Phys. Rev. Letters*, **41**, 1544.
Mészáros, P., and Ventura, J. 1979, *Phys. Rev. D*, **19**, 3565.
Mihalas, D. 1978, *Stellar Atmospheres* (2d ed.; San Francisco: Freeman).
Nagel, W. 1980, *Ap. J.*, **236**, 904.
———. 1981*a*, *Ap. J.*, **251**, 278.
———. 1981*b*, *Ap. J.*, **251**, 288.
Nagel, W., and Ventura, J. 1983, *Astr. Ap.*, **118**, 66.
Pavlov, G. G., Shibanov, Yu. A., and Yakovlev, D. G. 1980, *Ap. Space Sci.*, **73**, 33.
Pravdo, S. H., and Bussard, R. W. 1981, *Ap. J. (Letters)*, **246**, L115.
Pravdo, S. H., Bussard, R. W., Becker, R. H., Boldt, E. A., Holt, S. S., and Serlemitsos, P. J. 1978, *Ap. J.*, **225**, 988.
Rose, L. A., Pravdo, S. H., Kaluzienski, L. J., Marshall, F. E., Holt, S. S., Boldt, E. A., Rothschild, R. E., and Serlemitsos, P. J. 1979, *Ap. J.*, **231**, 919.
Soffel, M., *et al.* 1983, *Astr. Ap.*, **126**, 251.
Sunyaev, R. A., and Titarchuk, L. G. 1980, *Astr. Ap.*, **86**, 121.
Trümper, J., Pietsch, W., Reppin, C., Voges, W., Staubert, R., and Kendziorra, E. 1978, *Ap. J. (Letters)*, **219**, L105.
Ventura, J. 1979, *Phys. Rev. D*, **19**, 1684.
Ventura, J., Nagel, W., and Mészáros, P. 1979, *Ap. J. (Letters)*, **233**, L125.
Voges, W., Pietsch, W., Reppin, C., Trümper, J., Kendziorra, E., and Staubert, R. 1982, *Ap. J.*, **263**, 803.
Wang, Y.-M., and Frank, J. 1981, *Astr. Ap.*, **93**, 255.
Wasserman, I., and Salpeter, E. 1980, *Ap. J.*, **241**, 1107.
Wheaton, Wm. *et al.* 1979, *Nature*, **282**, 240.
White, N. E., Swank, J. H., and Holt, S. S. 1983, *Ap. J.*, **270**, 711.
Yahel, R. 1979, *Ap. J. (Letters)*, **229**, L73.
———. 1980, *Astr. Ap.*, **90**, 26.

PETER MÉSZÁROS: Astronomy Department, The Pennsylvania State University, 525 Davey Lab, University Park, PA 16802

WERNER NAGEL: Max-Planck-Institut für Astrophysik, Karl-Schwarzschildstr. 1, 8046 Garching, West Germany